# Preparation and characterization of cockle shell aragonite nanocomposite porous 3D scaffolds for bone repair

**7 authors**, including:

Saffanah Mahmood
University of Mosul
**32** PUBLICATIONS **175** CITATIONS

Md Zuki Abu Bakar
Universiti Putra Malaysia
**158** PUBLICATIONS **2,417** CITATIONS

Intan Shameha Abdul Razak
Universiti Putra Malaysia
**37** PUBLICATIONS **205** CITATIONS

Loqman Mohamad Yusof
Universiti Putra Malaysia
**55** PUBLICATIONS **690** CITATIONS

Some of the authors of this publication are also working on these related projects:

MAMMALIAN DEVELOPMENTAL ANATOMY View project

Toxicity View project

# Preparation and characterization of cockle shell aragonite nanocomposite porous 3D scaffolds for bone repair

Saffanah Khuder Mahmood[a,b,*], Md Zuki Abu Bakar Zakaria[a,c,*],
Intan Shameha Binti Abdul Razak[a], Loqman Mohamed Yusof[d], Alhaji Zubair Jaji[a], Isa Tijani[c],
Nahidah Ibrahim Hammadi[a]

[a] Department of Veterinary Preclinical Sciences, Faculty of Veterinary Medicine, Universiti Putra Malaysia (UPM), 43400 Serdang, Selangor Darul Ehsan, Malaysia
[b] Department of Veterinary Anatomy, Faculty of Veterinary Medicine, University of Mosul, Mosul, Iraq
[c] Laboratory of Molecular Biomedicine, Institute of Biosciences, Universiti Putra Malaysia (UPM), 43400 Serdang, Selangor Darul Ehsan, Malaysia
[d] Department of Companion Animal Medicine and Surgery, Faculty of Veterinary Medicine, Universiti Putra Malaysia (UPM), 43400 Serdang, Selangor Darul Ehsan,
Malaysia

## ABSTRACT

The demands for applicable tissue-engineered scaffolds that can be used to repair load-bearing segmental bone defects (SBDs) is vital and in increasing demand. In this study, seven different combinations of 3 dimensional (3D) novel nanocomposite porous structured scaffolds were fabricated to rebuild SBDs using an extraordinary blend of cockle shells ($CaCo_3$) nanoparticles (CCN), gelatin, dextran and dextrin to structure an ideal bone scaffold with adequate degradation rate using the Freeze Drying Method (FDM) and labeled as 5211, 5400, 6211, 6300, 7101, 7200 and 8100. The micron sized cockle shells powder obtained (75 μm) was made into nanoparticles using mechano-chemical, top-down method of nanoparticles synthesis with the presence of the surfactant BS-12 (dodecyl dimethyl bataine). The phase purity and crystallographic structures, the chemical functionality and the thermal characterization of the scaffolds' powder were recognized using X-Ray Diffractometer (XRD), Fourier transform infrared (FTIR) spectrophotometer and Differential Scanning Calorimetry (DSC) respectively. Characterizations of the scaffolds were assessed by Scanning Electron Microscopy (SEM), Degradation Manner, Water Absorption Test, Swelling Test, Mechanical Test and Porosity Test. Top-down method produced cockle shell nanoparticles having averagely range $37.8 \pm 3$–$55.2 \pm 9$ nm in size, which were determined using Transmission Electron Microscope (TEM). A mainly aragonite form of calcium carbonate was identified in both XRD and FTIR for all scaffolds, while the melting ($T_m$) and transition ($T_g$) temperatures were identified using DSC with the range of $T_m$ 62.4–75.5 °C and of $T_g$ 230.6–232.5 °C. The newly prepared scaffolds were with the following characteristics: (i) good biocompatibility and biodegradability, (ii) appropriate surface chemistry and (iii) highly porous, with interconnected pore network. Engineering analyses showed that scaffold 5211 possessed 3D interconnected homogenous porous structure with a porosity of about 49%, pore sizes ranging from 8.97 to 337 μm, mechanical strength 20.3 MPa, Young's Modulus $271 \pm 63$ MPa and enzymatic degradation rate 22.7 within 14 days.

## 1. Introduction

Recently, biomedical approaches that have involved in repairing and restoring the functions of damaged tissues are categorized under tissue engineering field. Of all bone, tissue engineering is one of the promising fields that aim to create biological replacements that have the ability to restore, repair, maintain or improve tissue functions. The steps often start with manipulating and manufacturing of an appropriate three dimensional (3D) porous scaffold suitable for bone tissue regeneration. However, scaffold modifications may be the best way to accelerate degradation, for instances, adding ceramic particles to increase the surface area that is available for hydrolysis to enhance functional repair of segmental defects [1,2]. There are many types of biomaterials that present endless opportunities for innovations of novel matrix or a substrate for cell seeding [3,4]. These biomaterials serve as extracellular matrix (ECM) capable of supporting the new bone morphogenesis [5,6]. Bone is a self-repairing organ that has the ability to adapt its mass, form and properties in response to changes, such as mechanical necessities, and endures specific physical action in life without breaking or causing pain [7]. These bio-capabilities of the bone come from the fact that bone is a living organ and contain cells that activate renewal and repair capabilities. It is made up of organic and inorganic (mineral) materials. The organic substance is concentrated in the bone matrix that consists mostly of 90% collagen fibers and other non-collagenous proteins. The inorganic substance of the bone is a calcium phosphate so called hydroxyapatite (HA), $Ca_{10}$ $(PO_4)_6(OH)_2$. The HA minerals is considered to fill the places between the collagen fibrils. The mechanical properties of any bone come from the impregnation process of the soft organic substances with HA minerals which are firm and brittle [8].

A scaffold is basically an extracellular matrix that offers a three dimensional structure capable of performing significant function. This practicability is due to a near-net-shape structure of the scaffold that guarantees ample porosity with appropriate pore size and interconnections in order to permit sufficient transportation and migration of cells, nutrients, metabolites, signal molecules as well as sufficient vascularization to nurture the new tissue growth [12,9]. The concept of bone tissue engineering is to develop and manufacture a biological substitutes (3D scaffolds) that enable the replacing of lost or damage bone caused by disease or trauma [6]. Up to date, bone replacement therapy includes autografts, allografts or xenografts [13,14]. Autografts can be engineered and produced either by culturing autologous cells in vitro guided by a scaffold or by implanting a cellular scaffold in vivo and letting the patient's cells to restore the bone tissue guided by the scaffold. It is preferred that the scaffold degraded at a certain time in harmony with tissue restoration time that means as soon as the tissue has developed the scaffold no longer exists and the newly developed tissue as functional as the lost tissue [15,5]. Such a scaffold must be created from biocompatible material with sufficient physical and mechanical properties as well as having no immunological or clinically foreign body reaction [16,4].

The materials of any scaffold must fulfill the following requirements: "1) biocompatibility 2) sterilizability 3) suitable physical characteristics (mechanical properties) 4) manufacturability 5) biodegradability 6) high porosity with interconnected network of pores and surface chemistry that promotes suitable regulation of cell activities such as a) cell adhesion b) proliferation c) migration and d) differentiation" [17]. There are many substances that have similarity to the bone structures that can be used to manufacture scaffolds to be used for bone tissue regeneration. Of all, natural coral (NC) has been used as a bone graft replacements due to its similar composition of bones. The NC can be transformed into structurally like porous HA via the hydrothermal exchange response. Hence, the mean diameter of the coral pore is 200 μm (190–230 μm) [15].

The basic difference between HA and NC is that the latter is biodegradable and HA is not. Both NC and HA are well known to be osteoconductive, biocompatible and very inert [18,19]. Ever since 1980, natural corallines of calcium carbonate ($CaCO_3$) and its transformed Hydroxyapatite, $Ca_{10}$ $(PO_4)_6(OH)_2$, have been widely used as a replacement biomaterial for bone grafts [15,18]. Moreover, quite a number of biomaterials have been investigated as candidates for bone graft alternatives, including animal bone, chitosan, coral exoskeletons and nacreous materials [2,20]. Best results are obtained with natural biomaterials due to better cell attachment, differentiation and function [21].

The cockle shell consists of about 96% $CaCO_3$ whilst other components include organic substances and other oxides like $SiO_2$, MgO and $SO_3$ [22,23]. The $CaCO_3$ has three polymorphs which are the calcite, aragonite and vaterite. Studies have moreover shown that the denser aragonite is an appropriate biomaterial because of its capability to be incorporated and replaced by bone tissues [24–27]. The significant characteristics of an ideal bone implant material are: "i) Biocompatibility ii) Mechanical strength and iii) Safety" [28,6]. The mixture of organic and inorganic resources provides a suitable different choice to mix the best properties of each stage and overcoming a lot of their weaknesses when used as standardized materials [29]. In past 10 years, the cockle shells powder was used to fabricate a novel porous scaffold. The relevance of this substance for manufacturing bone graft replacement comes from previous study conducted by Zuki et al. [22]. The study reported that cockle shells and coral exoskeletons have similar mineral and physicochemical characteristics [22,23,30,33]. Based on this previous study, it was recommended that the cockle shells can be used as good optional biomaterial for bone replacement in organization of bone defects. Gelatin plays a crucial role in the cockle shells research. It has been used widely in tissue engineering scaffolds due to its properties and has biological functions intact as its natural shape collagen such as biocompatibility and physical properties [31]. The aim of this study is to produce, and assess the morphological, physicochemical and mechanical properties of novel aragonite $CaCO_3$ nanoparticles, gelatin, dextran and dextrin derived scaffold as a potential bone matrix for tissue engineering and strengthening material.

## 2. Materials and methods

### 2.1. Cockle shells nanoparticles powder preparation

The cockle shells powder was prepared following the method described by Zuki et al., [22]. However, some modifications were made to obtain the best results. The shells were dried in oven (Memmert, UM 500, Germany) at 50 °C for 5–7 days, ground using stainless steel blender (Good and Well®, Taiwan) and sieved through 75 μm sieve (Endecotts Ltd, London, England). The micron sized powder was further dried in the oven (Memmert, UM 500, Germany) at 50 °C for 5 days and kept in air tight polyethylene plastic bag (JP Packaging) until used. The obtained micron sized powder 75 μm was transformed into nanoparticles using a mechano-chemical method in the presence of surfactant BS-12 (dodecyl dimethyl bataine) that was obtained from Sigma-Aldrich (Steinheim, Germany). Briefly, mechanical stirring of the 2 g of 75 μm powder with the 50 mL deionized water (DW) (HPLC-grade of resistance > 18 MΩ obtained from a MilliRO6 plus Milli-Q-Water System (Organex) and 0.5 mL of surfactant BS-12 at 1000 rpm at room temperature for 90 min using the heating homogenize stirrer machine (Wise Stir® Heating Multiple Stirring). The resultant slurry was then filtered using filter paper of size 12.5 cm (Filtres Fioroni, China) and dried at 80 °C overnight then stored at 50 °C in a sterile container prior to use.

### 2.2. Development of the scaffolds

Three specific natural materials namely gelatin, dextran and dextrin, were mixed together with the cockle shells nanoparticles

powder ($CaCO_3$) to formulate the scaffolds. Seven different formulae of the scaffolds were prepared using the following combinations:

**Scaffold 5211:** cockle shells nanoparticles 50%, gelatin 25%, dextran 10%, and dextrin 15%.
**Scaffold 5400:** cockle shells nanoparticles 50%, gelatin 40%, dextran 5%, and dextrin 5%.
**Scaffold 6211:** cockle shells nanoparticles 60%, gelatin 20%, dextran 10%, and dextrin 10%.
**Scaffold 6300:** cockle shells nanoparticles 60%, gelatin 30%, dextran 5%, and dextrin 5%.
**Scaffold 7101:** cockle shells nanoparticles 70%, gelatin 15%, dextran 5%, and dextrin 10%.
**Scaffold 7200:** cockle shells nanoparticles 70%, gelatin 20%, dextran 5%, and dextrin 5%.
**Scaffold 8100:** cockle shells nanoparticles 80%, gelatin 10%, dextran 5%, and dextrin 5%.

The numbers 5211, 5400, 6211, 6300, 7101, 7200 and 8100 represent the percentages of cockle shells nanoparticles powder, gelatin, dextran and dextrin respectively, and the scaffolds were prepared by deep freezing method. Combination of the three materials (gelatin, dextran, dextrin) was first dissolved in hot deionized water at 70 °C for 90 min using the heating homogenize stirrer machine (Wise Stir® Heating Multiple Stirring) at 400 rpm and the cockle shells nanoparticles powder was added to the mixture and stirred until a uniformly smooth slurry was achieved. The combination was poured into a cylindrical mold of aluminum foil 4 cm height x 1 cm diameter, allowed to set slightly before being transferred to −20 °C for 24 h then transferred to the deep freezer at −80 °C and the scaffolds was later freeze dried in a freeze drier (LABCONCO Freezon[6] USA) for lyophilization till it is completely dried for 4 days at −50 °C, and later kept in a sterile container before future use (Fig. 1) [30,32,33]. The experimental were repeated minimum of three times to ensure a proper reliability and observation.

### 2.3. Scaffold characterization

#### 2.3.1. Scanning Electron Microscopy (SEM) study

Examination of prepared scaffolds was done by Scanning Electron Microscopy (JEOL JSM 6400 SEM ATTACHED WITH EDX, Germany). Cutting of the scaffolds into smaller circular and longitudinal sections was done and sent to the Electron Microscopy Unit, Institute of Bioscience, Universiti Putra Malaysia for SEM analysis. The samples were fixed on stubs at various angles and sputter coated with gold (BAL-TEC SCD 005) prior to studies on electron conductivity, Microstructural characterization and average pore diameter of measurement based on 300 measurements that was taken at different positions on the micrograph picture from six replicates [30,32,33].

#### 2.3.2. Porosity study

Porosity of the organized scaffolds was examined via fluid dislocation using ethanol; this method was adopted from Shahini et al., [34]. The scaffolds were cut into smaller circular discs, 1 cm in diameter and 1 cm thickness. Initial dry weight ($W_d$), the radius (R) and the thickness (T) of 6 samples per scaffold were calculated preceding immersion. Samples were later dipped in 20 mL ethanol alcohol and subsequently treated with an evacuation-repressurization system until no more bubbles came out of the specimens and left in ethanol for 48 h, to allow thorough saturation, and were weighed and recorded as ($W_w$). Scaffold porosity was calculated according to the formula below.

**Porosity Percentage** $= (W_w − W_d)/P_{et} \times \pi R^2 T \times 100\%$

While ($P_{et}$) represent the density of ethanol.

#### 2.3.3. Swelling study

The swelling study was conducted following Soumya et al. [35] method. This measured the absorption/diffusion of the nutrients into the scaffolds, vital for cell viability and growth. The swelling test determined the percentage of medium uptake by each scaffold. Six samples of each type of the fabricated scaffolds were used in this study; the weights of each sample were measured before and after soaking in
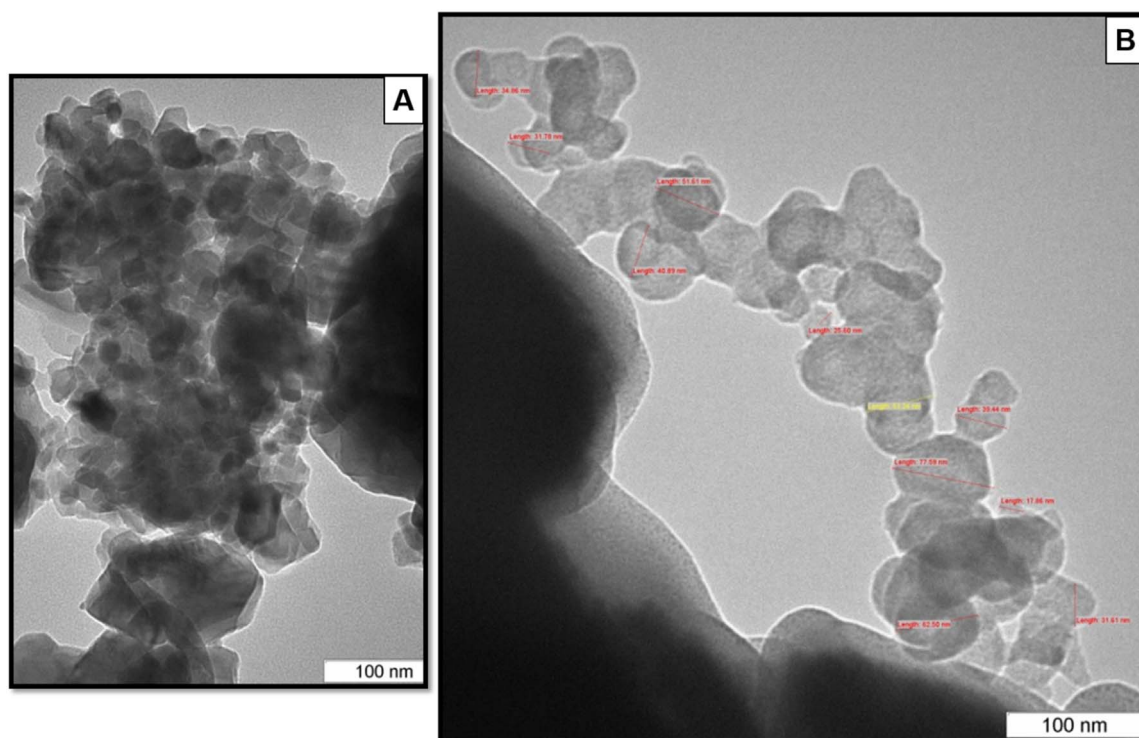


**Fig. 1.** Photographs show the shape and the size of cockle shells nanoparticles using TEM, (A and B), 100 nm.

phosphate buffer solution (PBS) pH 7.4 for 10 min. The difference between the weight of wet and dry scaffolds denotes the quantity of PBS solution from which the percentage of medium uptake was calculated according to the following formula:

**Percentage of medium uptake $= (W_2 - W_1)/W_1 \times 100\%$**

where, $(W_1)$ is the initial sample weight before immersion (dry) and $(W_2)$ is the sample weight after immersion (wet). The above process was repeated after drying the same scaffolds samples for another 10 min. The finest sample was recognized based on the comparison between the scaffolds for the first and the second percentage of PBS absorption.

### 2.3.4. Water absorption study

Water absorption study was carried out using six samples of each type of scaffold. The weights of samples were measured before and after immersion in deionized water for 10 min. The difference between the weight of wet and dry samples denotes the quantity of absorbed water from which the percentage of absorbed water were calculated according to the following formula:

**Percentage of medium uptake $= (W_2 - W_1)/W_1 \times 100\%$**

where, $(W_1)$ is the initial sample weight before soaking (dry), and $(W_2)$ is the sample weight after soaking (wet). The above method was repeated after drying the scaffolds for another 10 min. The best sample was recognized based on the comparison between the scaffolds samples for the first and the second percentage of water absorption.

### 2.3.5. Degradation study

Degradation of the 3D nanocomposite scaffolds was studied in PBS solution pH 7.4 using two approaches. The first approach enzymatic method entailed the study of the degradation rate using lysozyme, in adoption of [36] method. Six samples measuring 1 cm in diameter and 1 cm in thickness each were tested from each scaffold type. The samples were immersed in PBS solution containing 10,000 U/mL lysozyme at 37 °C for 14 days. The liquid was changed every 3 days to guarantee constant enzyme activity. Initial weights of each sample of the scaffolds were recorded as $W_0$. The samples were removed after 14 days and freeze dried for 4 days at $-50$ °C. The samples were then weighed and the dry weight was recorded as $(W_1)$. The degradation percentage was then calculated according to the following formula:

**Degradation $\% = (W_0 - W_1)/W_0 \times 100\%$**

For the second semi-quantitative method, six samples measuring 1 cm in diameter and 1 cm in thickness each were collected from each scaffold type for the 14 days semi-quantitative experiment. Photographs were obtained at fixed time intervals to show the physical changes of the degrading scaffolds. During the degradation of the samples, the pH changes were also concurrently measured at changeable intervals.

For third semi-quantitative method this study adopted a direct visual examination method (by naked eye) to assess the degradation rate. At different periods of time, comparison of the scaffold condition by monitoring the changes in the scaffold dimensions soaked in special environment. Six samples were collected from each scaffold measuring 1 cm in diameter and 1 cm in thickness each were used for this 14 days semi-quantitative experiment. The samples were immersed in deionized water. The information provided by the degradation in PBS solution pH 7.4 using the two approaches and through the direct visual observation method was acceptable to judge the differentiation in degradation rates of different types of scaffolds with different manufactured components.

### 2.3.6. Mechanical strength study

Compressive mechanical strength and modulus of scaffolds were tested using an Instron 3365 mechanical tester (Instron 3365, 10 kN load-cells, Canton, MA, USA) with 10 kN load cells [9]. Six samples

were collected from each scaffold and prepared as circular discs of 1 cm in diameter and 1 cm thickness. The speed of a crosshead which used was 0.4 mm/min and the load was applied till the samples were compressed to approximately 100% of its original height. The stiffness of the scaffolds was assessed at the stress point region. The yield strength was taken to the yield point on stress-strain MPa.

### 2.3.7. Fourier Transform Infrared (FTIR) analysis

To find out the chemical functionality of the 3D nanocomposite scaffolds, the spectroscopic method utilizing a Fourier Transform Infrared (FTIR) spectrophotometer (Perkin Elmer) was used over the range of 400 cm$^{-1}$ to 4000 cm$^{-1}$. 1–2 g of samples was prepared and used through UATR methods.

### 2.3.8. Powder X-Ray Diffraction (PXRD) analysis

1–2 g of samples of each scaffold type were ground and used for this analysis. The analysis entailed performing wide-angle X-Ray Diffraction to differentiate the nature of amorphous and crystalline components of the samples at room temperature. All crystalline phases present were recognized using X-ray powder diffractometer (Shimadzu XRD-6000, Japan powder diffractometer) through the use of CuKα ($\lambda = 1.540562$ Å) at 40 kV and 30 mA [10]. The diffraction form was collected at a rate of scanning 0.02 degrees per second in 2θ at a range of 20° to 60° at 37 °C.

XPPA by Scherrer's formula to compare with the values obtained from TEM analysis results. The crystallite sizes Dv is an easy technique that openly distinguishes between strain induced and size induced peak extending through considering the peak length as a function of 2θ [11].

### 2.3.9. Differential Scanning Calorimetry (DSC) analysis

Differential Scanning Calorimetry (DSC) was performed on scaffold samples to examine their thermal characteristics. The thermal change of the scaffolds powder developed from different combinations was analyzed using differential scanning calorimeter (METTLER TOLEDO DSC822e Switzerland). About 1–2 g of samples of each scaffold were grounded, prepared and used for this analysis. The sample powders were scanned at room temperature. Samples were heated up to 250 °C at the rate of 10 °C/min, held isothermally for five minutes and cooled again to 25 °C during each cycle. During the first cycle, the heat of the melting temperature, $(T_m)$, was recorded in order to find out the crystallinity. The minimum of the melting peak was defined of melting temperature. During the second cycle, the glass transition temperature $(T_g)$ was determined as the inflection point of the glass transition.

### 2.3.10. Statistical analysis

First of all, the quantifiable outcomes were evaluated using Explore for Normality of data then One-Way Analysis of Variance (ANOVA) and Kruskal-Wallis Test. The results were shown as Mean ± Standard Error (SE). Post Hoc Test were calculated for significant values $p < 0.05$ using Tukey's Multiple Comparison Test. All descriptive and inferential statistical analyses was conducted using Excel version 2013, SPSS version 21.0, 22.0 and 23.0 and SAS version 9.4.

## 3. Results

### 3.1. Characterization of cockle shells nanoparticles

The TEM revealed aragonite calcium carbonate nanoparticles (ACN) with a range size of 37.8 ± 3–55.2 ± 9 nm (Fig. 1 and Table 5). There was no change in the elemental compositions of the obtained cockle shells nanoparticles post synthesis using of BS-12. This reflects the surfactant role of BS-12 in the break of the larger sized aragonite rods into smaller spherical ones.
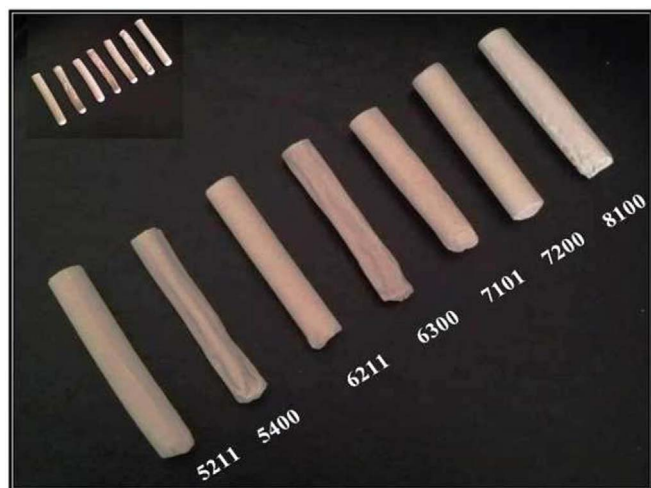
**Fig. 2.** Photograph shows scaffolds after drying in the freeze dryer machine, which ready to be used for studying the scaffolds characterization.

### 3.2. Characterization of scaffolds

Fig. 2 shows the developed scaffolds in different compositions of gelatin, dextran, and dextrin and ACN. The scaffolds formed were found to be stiff in structure. The whiteness of the scaffolds varies based on the percentage of the ACN. The higher the ACN powder percentage the whiter scaffold will appear. The scaffolds were also found to be hard enough to bear up the physical manual compression in dry state, which allows it to be simply handled and cut into desired sizes for further studies.

#### 3.2.1. Scanning Electron Microscopy (SEM) study

The scaffolds that were prepared by freeze dry method gave rise to structures that consisted of open networks of pores, with pore sizes that ranged from 8.97 to 526 μm (Table 1). The pores showed a high degree of interconnection, which is very crucial for cell seeding and growth. With this method it was possible to control the porosity percentage and the pores size. SEM analysis showed excellent micro pores structures with sizes varying from 9 to 526 μm. However, the scaffolds 5400 and 7101 showed an extremely wide pore structures ranging from 11.7 to 478 μm and 16.8 to 526 μm respectively (Figs. 3–6 and Table 1). The pores were round in structure with diameters ranging between 56.84 and 108.22 μm. However the group of scaffolds that have higher concentration of ACN showed higher calcium carbonate crystallites deposited on the surface of the gelatin, dextran and dextrin polymer. Table 1 shows the summary of pore diameter range and mean pore size of each scaffold. Noteworthy to mention that there was a negative relation between the pore size and the percentage of ACN except for the scaffold 7101.

**Table 1**
Summary of pores diameters of each scaffold, (Range μm), (Mean ± SE), (a*) means significant difference were observed between the scaffolds at $p < 0.05$.

| Name of scaffold | Range of pores diameter | Mean of pores diameter |
| --- | --- | --- |
| Scaffold 5211 | 8.97–337 μm | 71.27 μm ± 3 b |
| Scaffold 5400 | 11.7–478 μm | 77.27 μm ± 7 b |
| Scaffold 6211 | 16.5–435 μm | 94.71 μm ± 2 c |
| Scaffold 6300 | 12.4–358 μm | 92.32 μm ± 6 b |
| Scaffold 7101 | 16.8–526 μm | 108.22 μm ± 8 d |
| Scaffold 7200 | 15.5–348 μm | 56.84 μm ± 3 a* |
| Scaffold 8100 | 16.9–225 μm | 59.89 μm ± 2 a* |

The means with similar letters are not significantly different.

#### 3.2.2. Porosity study

Scaffolds from different compositions showed significant differences at $p < 0.05$ in the porosity percentage between 33% and 97% (Fig. 7). The results also showed that the higher percentage of ACN powder, in a scaffold, the higher was its porosity percentage.

#### 3.2.3. Swelling study

Fig. 8 shows the percentage of medium uptake of each scaffold at a given period obtained by manipulative changes in scaffold weight. Scaffold 5400 showed the lowest PBS solution absorbing ability at 34.92 ± 3% in the first 10 min, whilst scaffold 7200 scaffolds showed the highest absorbing capability at 65.54 ± 8%. Scaffold 6211 showed the lowest PBS solution absorbing ability at 23.49 ± 2% in the second 10 min, whereas scaffold 6300 showed the highest absorbing capability at 42.62 ± 2%. The PBS solution ability of the seven scaffolds were found to vary between 35% and 66% for first 10 min and between 23% and 43% for second 10 min with significant differences between the scaffolds for first 10 min at $p < 0.05$. No significant differences was observed between the scaffolds for second 10 min at $p > 0.05$.

#### 3.2.4. Water absorption study

Fig. 8 shows the outcome of water absorption test for different composition of scaffolds. After the first 10 min, the scaffold 7101 and 8100 were more resistant than the other scaffolds. The second 10 min of immersion was done after the scaffolds were left to dry. The percentage of water absorption had dropped in scaffolds 7101 and 8100. All types of scaffolds showed significant difference between the scaffolds for the first and second 10 min at $p < 0.05$.

#### 3.2.5. Degradation study

The degradation study of the scaffolds was carried out using an enzymatic way as well as two semi-quantitative methods for a time period of 14 days. The results show that scaffold 6211 showed higher degradation rate at 67% and the scaffold 5211 showed lower degradation rate at 15% compared to other scaffolds (Fig. 8). The degradation rate of the scaffolds was different from one to other, the scaffold 5400 was 24%, 6300 was 28.6% and 7200 was 28.7% degraded at the day 4 of the test, whilst scaffold 7101 and 8100 showed 31% and 19.5% degradation percentage respectively, which degraded at day 6 of the test, and scaffold 6211 showed higher degradation at 67% at day 7 of the test. Whereas, scaffold 5211 showed lower degradation at 15% at day 10 of test respectively (Fig. 8 and Table 2). The degradation development displayed by the scaffolds was found to be associated with the concentration of ACN powder as well as the concentration of gelatin within the same scaffold. Low content of gelatin showed higher degradation rate except for scaffold 6211 that has showed higher degradation with high concentration of gelatin (Figs. 8–10 and Table 2). Moreover, there was no significant differences in the degradation percentage of all the scaffolds studied at $p > 0.05$.

Table 2 shows the summary of degradation periods from 6 replicates of each scaffold using PBS solution. The results from scaffold degradation periods showed different model of degradation as observed throughout the enzymatic degradation studies with scaffolds consisting higher concentration of ACN powder showing higher degradation rate. Scaffold 7101, 7200 and 8100 showed faster breaking of the scaffold structure by day 2 and wholly lost its structure by day 4. Comparatively scaffold 5400, 6211 and 6300 showed a moderate degradation approach with small surface defects and mild fissure within day 6. Figs. 11 and 12 show the photographic images of the disintegrating scaffolds captured at two intervals.

#### 3.2.6. pH changes during degradation study

Table 3 shows the changes in pH during the experimental period. There were significant changes in the pH within the scaffold groups, in addition significant changes between groups were observed after 24, 288 and 336 h at $p < 0.05$. No significant changes were seen between
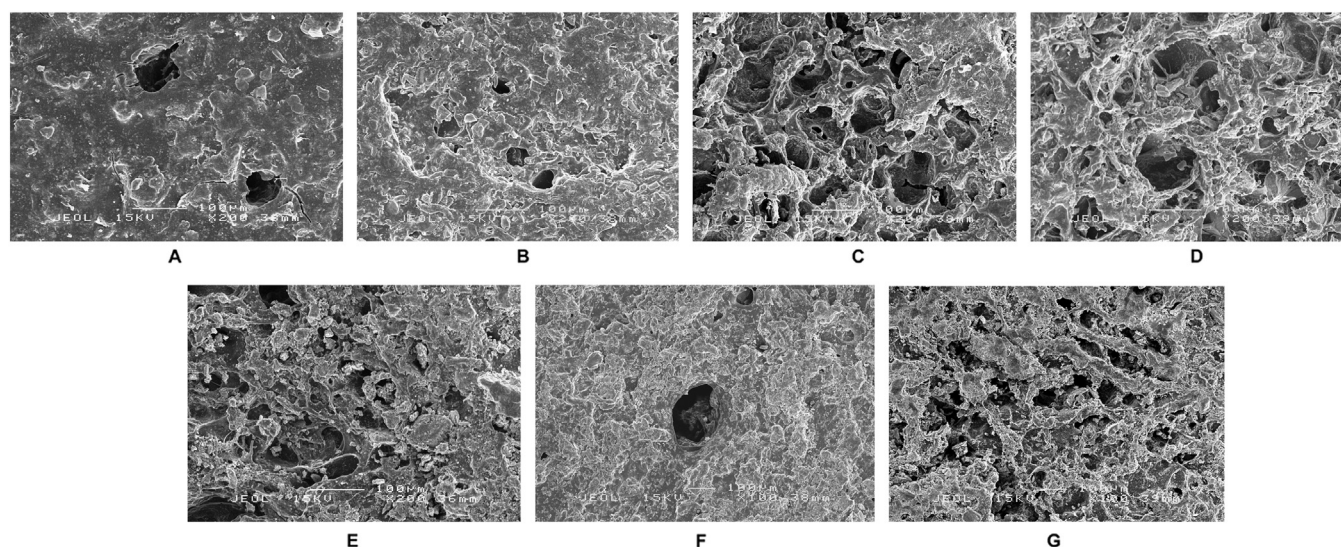
**Fig. 3.** Photographs (A, B, C, D, E, F and G) show the superficial structure of scaffolds (5211, 5400, 6211, 6300, 7101, 7200 and 8100) using Scanning Electron Microscope. A, B, C, D and E, 200x and F and G, 100x.

groups after 72 and 168 h at $p > 0.05$. There was a significant increase in the pH in scaffold 5211 compared to other scaffolds at the end of the study period at $p < 0.05$. An increased pH to a basic condition was observable within all the concentrations of ACN powder with a maximum pH of 9.09 in scaffold 5211. Scaffold 5400 and 6211 achieved a maximum pH of 8.45 and 8.72 correspondingly, while scaffold 6300 showed a maximum increase in pH values of 8.34, and scaffolds 7101 and 7200 showed same maximum increase in pH value of 8.39, and the scaffold 8100 showed a maximum increase in pH values of 8.25.

### 3.2.7. Mechanical strength study

The stiffness and yield were determined from the compression test. Fig. 13 shows the compression strength and Young's Modulus of the scaffolds tested under a 10 kN load. The compression strengths of scaffold 5211 and 5400 were $20.31 \pm 4$ MPa and $18.54 \pm 6$ MPa respectively and found to be significantly higher compared to the other scaffolds at $p < 0.05$. Scaffold 8100 displayed the lowest compression strength at $3.55 \pm 0.3$ MPa in spite of a remarkable tendency of increase in the compression strength with the ACN powder composition

and increase in gelatin composition. The Young's Modulus of scaffold 5211 and 6211 were $270.635 \pm 63$ MPa and $240.208 \pm 103$ respectively and found to be higher compared to the other scaffolds. Scaffold 7200 displayed the lowest Young's Modulus at $103.52 \pm 30$ MPa. Scaffolds from different compositions showed significant differences in the compression strength at $p < 0.05$ and no significant differences in the Young's Modulus at $p > 0.05$.

### 3.2.8. Fourier Transform Infrared (FTIR) analysis

The FTIR spectra of the scaffolds were showed in Fig. 14. In all scaffolds, a similar pattern of spectra was observed with slight different in scaffold 8100. The major bands of the FTIR spectra from the analysis were observed in Table 4. The bands represent some major groups representing the stretching of hydroxyl, carboxyl, amide and amine bands. The presence of C-H groups and C-O groups of the gelatin, dextran, dextrin and aragonite bands of ACN powder are also reported.

### 3.2.9. Powder X-Ray Diffraction (PXRD) analysis

The XRD pattern of the prepared scaffolds is shown in Fig. 15. The X-Ray powder diffraction analysis is a sensitive test used for the
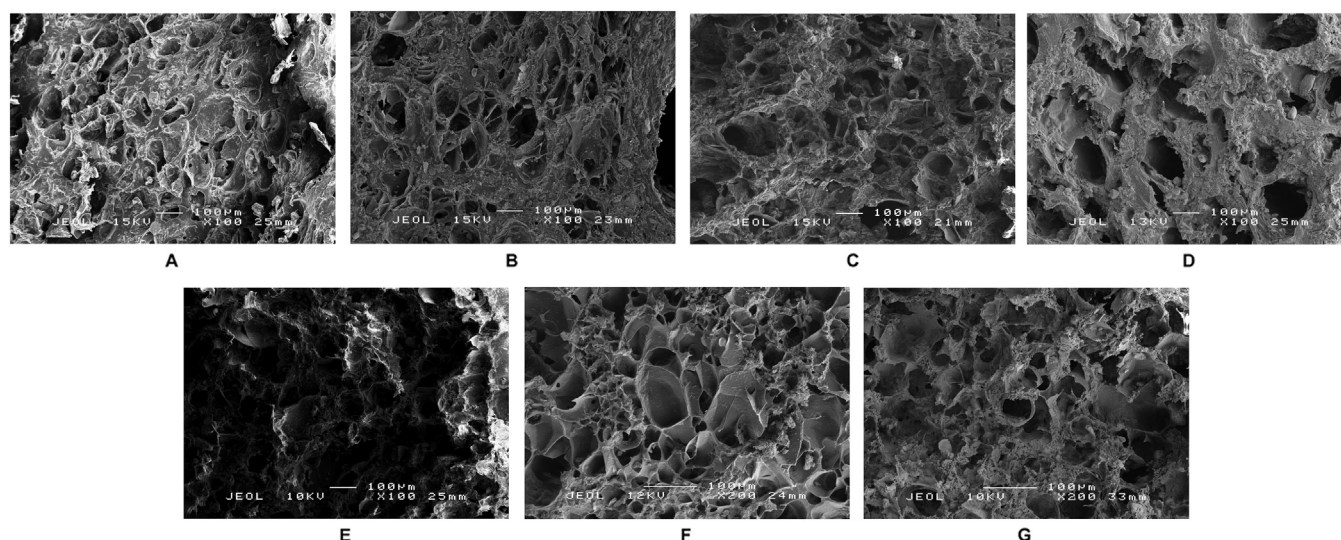


**Fig. 4.** Photographs (A, B, C, D, E, F and G) show the internal structure of the scaffolds (5211, 5400, 6211, 6300, 7101. 7200 and 8100) using Scanning Electron Microscope. A, C, E and G, longitudinal section, B, D and F, Cross section. A, B, C, D and E 100x., F and G, 200x.
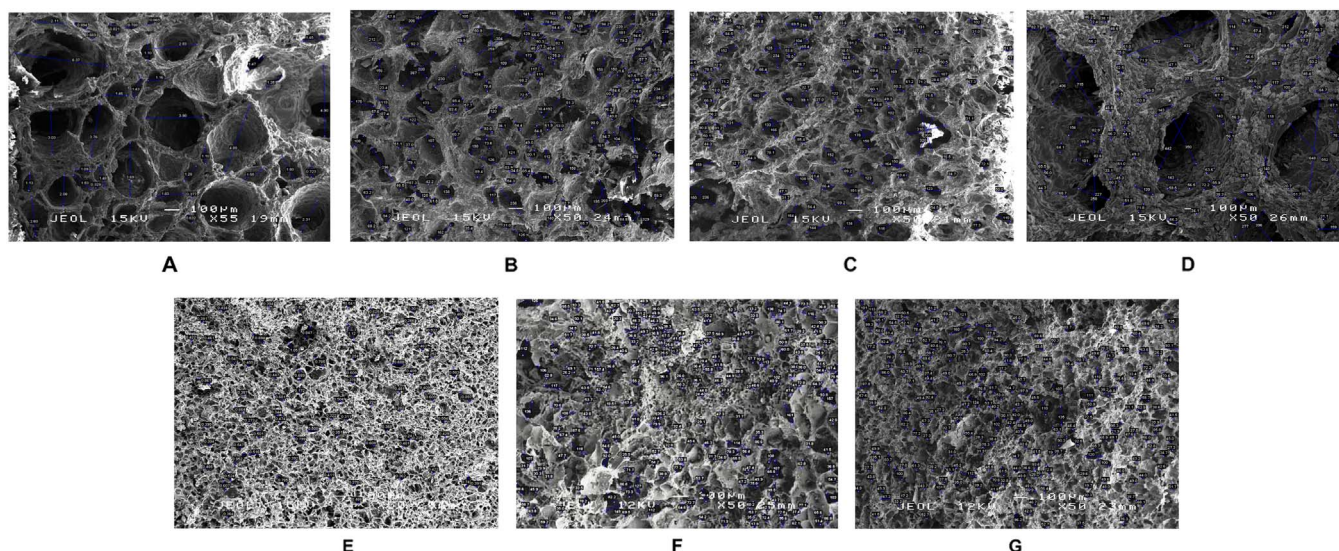
**Fig. 5.** Photographs (A, B, C, D, E, F and G) show the internal structure and pores diameter of the scaffolds (5211, 5400, 6211, 6300, 7101, 7200 and 8100) using Scanning Electron Microscope. A, C, D, E and G, cross section, B and F longitudinal section. 50x.

recognition of crystalline phases of inorganic compounds (Shimadzu XRD-6000 powder diffractometer using CuKα (λ = 1.540562 Å) at 40 kV and 30 mA). The scaffolds powders were sent to the Material Science Laboratory, Department of Chemistry, Faculty of Science (FOS), Universiti Putra Malaysia for XRD analysis. The x-ray powder diffractometer is a very useful analytical method that is based on the principle that X-Rays of wavelength that is known passes through a sample to be recognized in identifying the crystal configuration. The crystals lattice diffract the wave nature of the X-Rays giving a exceptional shape of peaks of 'reflections' at different viewpoints and of diverse strength, as light can be deflected by means of a rough suitably spaced shapes. According to Bragg principle, the deflected rays from atoms in succeeding planes cancel except they are in phase. Preparation of samples for XRD entailed packing about 2 g of scaffold powder to the holder through the use of a standard back fill technique appropriately secure adequately for it not to drop out throughout the 90ø tilt test. Crystallinity phases were determined with diffraction angles from 20° to 70° at 37 °C. Fig. 15 shows that the XRD absorption peaks in the scaffolds powders matched each other. This means that the crystalline quality of aragonite CaCO3 nanoparticles in these powders is main-
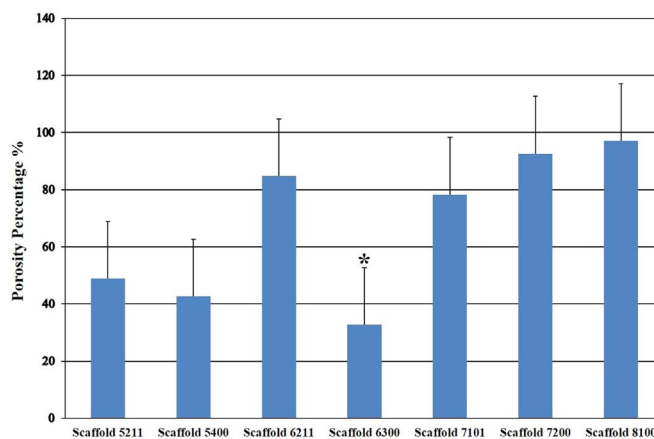


**Fig. 7.** The mean of porosity percentage of scaffolds tested through liquid displacement method. *Significant difference were observed between the scaffolds at p < 0.05.



**Fig. 6.** Photographs (A, B, C, D, E, F, G) show the internal structure and pores of the scaffolds (5211, 5400, 6211, 6300, 7101, 7200 and 8100) using Scanning Electron Microscope. A, B, E, F and G, longitudinal section, C and D, longitudinal section. 1000x magnification showing the presences of cockle shells nanoparticles powder crystallites depositions on the internal matrix.

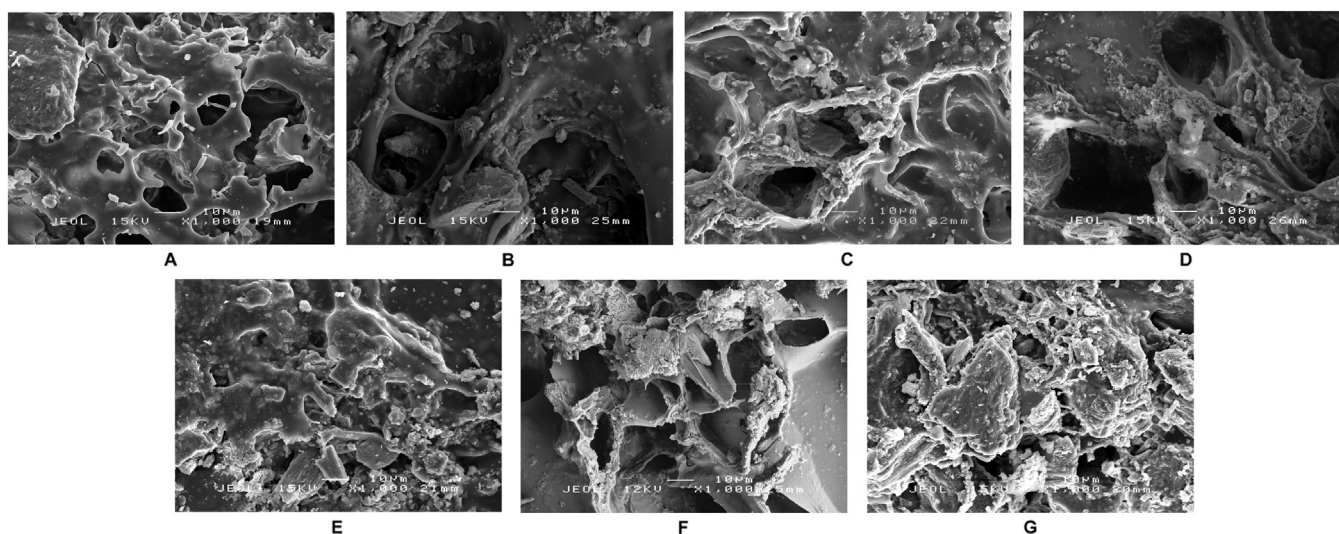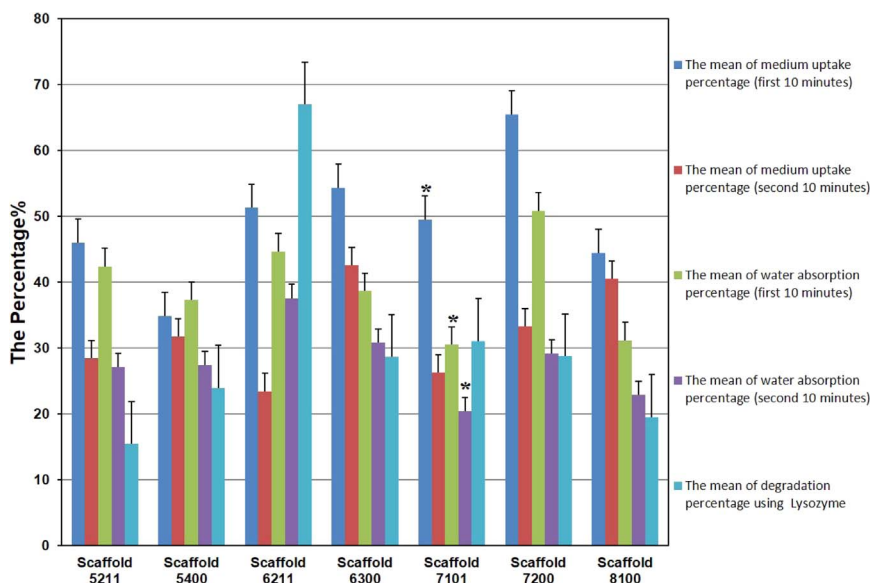**Fig. 8.** The mean of medium uptake percentage and the mean of water absorption percentage (first and second 10 min) and the mean of degradation percentage using Lysozyme. *Significant difference were observed between the scaffolds at $p < 0.05$.

tained throughout the process of scaffolds production. XRD absorption peaks in the ANC matched each other. Two prominent peaks were found each in ANC spectra. The first set of peaks were within $2\theta = 26.2°$ to $26.5°$ while the second set were within $2\theta = 33.1°$ to $33.2°$ and the third set were within $2\theta = 45.8°$ to $46.1°$. This means that the crystalline quality of ANC is maintained throughout the process of production. These findings are further supported by XRD diffractograms indicating presence of aragonite in the entire four samples as equated to a standard calcium carbonate diffractogram having peaks from the shell powders seen to matched closely to the aragonite phase of Joint Committee of Powder Diffraction Society (JCPDS) file no. 00-041-1475. The XRD investigation done showed essential information on mineral phase of the materials existing in the scaffolds. The obtained information from the spectrums established the presence of the distinctive peaks of aragonite. The powder X-ray diffraction (PXRD) and transmission electron microscopy (TEM) methods were used to investigate the phase configuration, the morphology and size of made CaCO3 powder. The isolated and ideal high strength diffraction peaks namely, (26.2), (26.3), (26.5), (33.1), (33.2), (45.8), (45.9), and (46.1) were selected for estimating the nanostructural parameters through several models using Scherrer's formula (Table 5).

The PXRD patterns of scaffolds powders are comparable and display numerous diffraction points that could be apportioned to sphere-shaped crystal structure. Furthermore, the diffraction points are distinctly wider signifying that the particles of prepared powder were in nanosize. Powder X-ray diffraction (PXRD) was utilized in limiting the composition and pureness of the produced CaCO3 nanoparticles. The PXRD patterns of scaffolds powders revealed typical peaks having high density between $2\theta$ of 26° and 46°.

### 3.2.10. Differential Scanning Calorimetry (DSC) analysis

Thermal characteristics of the scaffolds were analyzed using DSC scans as shown in Fig. 16. There was no crystallization peak during the first run, thus the percentage crystallinity was calculated only with the Heat of fusion $H_f$. Firstly heating rises from room temperature 25 °C to 250 °C at 10 °C/min. During this rise, the material displays information on its real physical and morphological condition. This rise was used to assess the Heat of fusion, $(H_f)$ and melting Temperature, $(T_m)$ of the materials. While, the second heating rise was used to calculate the glass transition Temperature, $(T_g)$ which is investigative of polymer chain length and thus polymer degradation. The DSC curve for scaffold 5211 showed a glass transition point for the non-cross linked sample at 232.58 °C. The heating of scaffolds results in a loss of the compound structure, and the temperature at which melting procedure occurs was a helpful tool to differentiate these powders preparations, and this transition can be observed by DSC. Endothermal reactions start between 62.41°C and 75.51 °C, depending on the powders resource, processing and pH. It can be seen that the thermal mark of the powder mix had a minimum melting peak at about 62.41, 63.04, 65.48 and 75.51 °C for scaffolds 8100, 7101, 6211 and 5211 correspondingly and the second minimum glass transition peak were between 230.69 and 232.58 °C.

## 4. Discussion

This study aimed at evaluating the gelatin, dextrin, dextran and ACN, as scaffold materials for bone tissue restoring applications, in addition to improving nanoparticles usage in scaffold design. The development and characterization techniques of a material are crucial pre-determining factors vital to its reliability in further assessments

**Table 2**
Summary of degradation period of each scaffold during degradation manner.

| The scaffold | Degradation using Lysozyme | Degradation using PBS | Degradation using DW |
|---|---|---|---|
| Scaffold 5211 | 10 days | 6 days | 14 days |
| Scaffold 5400 | 4 days | 5 days | 7days |
| Scaffold 6211 | 7 days | 5 days | 8 days |
| Scaffold 6300 | 4 days | 5 days | 8days |
| Scaffold 7101 | 6 days | 4 days | 7 days |
| Scaffold 7200 | 4 days | 4 days | 6 days |
| Scaffold 8100 | 6 days | 4 days | 7 days |

| Scaffold 5211 | Scaffold 5400 | Scaffold 6211 | Scaffold 6300 |

| Scaffold 7101 | Scaffold 7200 | Scaffold 8100 |

Fig. 9. Photographs show the degradation manner of each scaffold using Lysozyme after 24 h.

[32]. Dextran was chosen for this study because of its known resistant to both protein adsorption and cell adhesion. The quantity of dextran used in scaffold is a determinant of its porosity and interconnectivity [32]. More so; it is suitable to work with a scaffold that has explicit sites for cell recognition [37,38]. In our study lyophilization method produced scaffolds with brilliant porosity [39]. Heating was the main means of evaporation of water in this study which made the mixture concentrated and dense enough to entrap the air bubbles thus,

increasing the porosity after the mixture was dried. Similar results were reported by [39,40,41,32,42].

The SEM investigation of the developed scaffolds revealed that micro-pores with multiple sizes. The physical structure of this microporosity of the scaffolds was mainly attributed to air cavities. These supplied spaces to accommodate the effect of swelling on the scaffolds. This observation was similar to those of [41,32,30,33]. It was observed that the scaffolds have less than 50% porosity via liquid displacement



| Scaffold 5211 | Scaffold 5400 | Scaffold 6211 | Scaffold 6300 |

| Scaffold 7101 | Scaffold 7200 | Scaffold 8100 |

Fig. 10. Photographs show the degradation manner of each scaffold using Lysozyme after 7 days.

**Fig. 11.** Photographs show the degradation manner of each scaffold using PBS after 24 h.



**Fig. 12.** Photographs show the degradation manner of each scaffold using PBS after 3 days.

**Table 3**
The mean of pH during degradation period using PBS. (a*) means significant difference were observed between the scaffolds at $p < 0.05$.

| The scaffold | After 24 h | After 72 h | After 168 h | After 288 h | After 336 h |
|---|---|---|---|---|---|
| Scaffold 5211 | 7.27 ± 0.2 b | 7.16 ± 0.3 | 7.13 ± 0.1 | 7.29 ± 0.2 a* | 9.09 ± 0.1 b |
| Scaffold 5400 | 6.96 ± 0.1 a * | 7.14 ± 0.1 | 7.02 ± 0.1 | 7.33 ± 0.01 a* | 8.45 ± 0.1 a* |
| Scaffold 6211 | 7.06 ± 0.1 b | 7.22 ± 0.1 | 7.19 ± 0.2 | 8.29 ± 0.2 b | 8.72 ± 0.2 b |
| Scaffold 6300 | 6.97 ± 0.01 a * | 7.25 ± 0.4 | 7.15 ± 0.1 | 7.17 ± 0.02 a* | 8.34 ± 0.02 a* |
| Scaffold 7101 | 7.54 ± 0.02 b | 7.27 ± 0.1 | 7.20 ± 0.1 | 7.37 ± 0.1 a* | 8.39 ± 0.03 a* |
| Scaffold 7200 | 7.47 ± 0.03 b | 7.33 ± 0.1 | 7.25 ± 0.1 | 7.23 ± 0.1 a* | 8.39 ± 0.01 a* |
| Scaffold 8100 | 8.11 ± 0.01 c | 7.86 ± 0.1 | 7.15 ± 0.2 | 7.50 ± 0.1 a* | 8.25 ± 0.1 a* |

The means with similar letters are not significantly different.

method using ethanol. Nonetheless, scaffolds with higher ACN concentration showed a relatively higher porosity with maximum composition of ACN (scaffold 8100). Similarly, [30,33,35,43] reported the same results. This could be due to the water evaporation during lyophilization process. Evaporation created porous structures in the scaffolds due to the detachment of nanoparticles powder within the gelatin, dextrin and dextran matrices during freezing. The higher the ACN powder contents the higher the amount of aggregates detached within the gelatin, dextrin and dextran matrices [30,32,33].

A vital aspect that is negatively related to porosity is the mechanical characteristics of the scaffold. Porosity of a scaffold adversely affects its mechanical strength. Any increase in porosity often occurs as decrease in the mechanical strength of the scaffold. This flaw or undesired phenomenon is frequently appearing in polymer based scaffold, as developed in this study. Many studies have been reported on the enhancement of mechanical characteristics of scaffolds by integration of inorganic biological substances [44–47]. Gelatin, dextrin and dextran are known natural polymers that form a fragile hydrogel like scaffolds. The blend of ACN powder with gelatin, dextrin and dextran resulted in advanced nanocomposite scaffold with tremendously enhanced mechanical characteristics. The results from this study suggest a significant increase in both the mechanical characteristics and Young's Modulus of the scaffolds that were combined with ACN. It was observed that the mechanical properties of the scaffolds were positively related to the concentration of gelatin and dextrin content in scaffold compositions. This relation was obvious in scaffold 7101, 7200 and 8100 that showed a decrease in their mechanical strength and modulus regardless of having the highest content of ACN and lowest content of gelatin and dextrin. This is possibly was due to the increased porosity of scaffold 7101, 7200 and 8100 that have eventually resulted in decreasing their
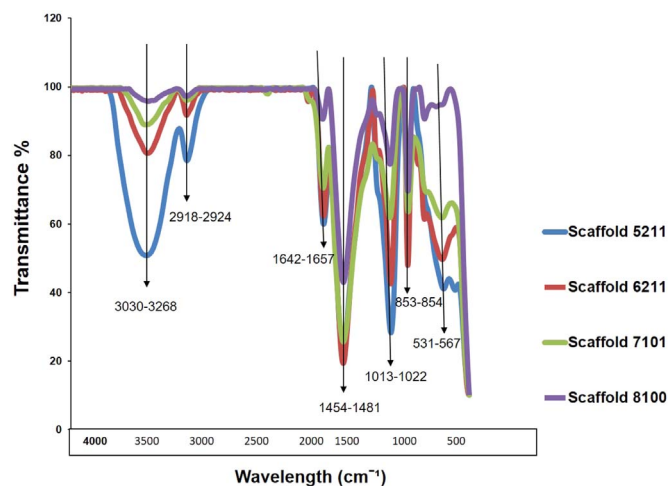


**Fig. 14.** FTIR spectra of scaffolds.

mechanical properties.

Spherical pores have good tendency to resist higher compression loads [43,44]. Some of the factors that scaffolds must have to control its mechanical properties are pore size and its interconnectivity [30,32,33,43,48]. In this study, scaffold 5211 demonstrated a good mechanical property that ranged between the hard bone structure of 271 ± 63 MPa with a compressive strength of 20.3 MPa making this combination the most suitable conditions of mechanical properties as earlier reported by [17,44,47]. Mechanical strength of nanocomposite scaffolds is believed to be added by strong ionic interaction that
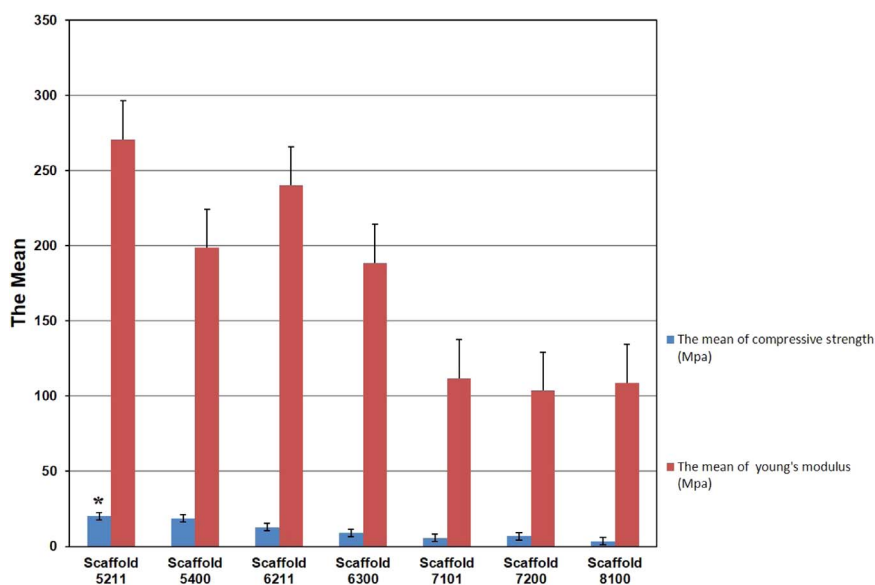


**Fig. 13.** The mean of compressive strength (MPa) and young's modulus (Mpa). *Significant difference was observed between the scaffolds at $p < 0.05$.

**Table 4**
Summary of major bands and intense peaks observed in the FTIR spectra (mean). (a*) means significant difference were observed between the scaffolds at $p < 0.05$.

| Scaffold 5211 | Scaffold 6211 | Scaffold 7101 | Scaffold 8100 |
|---|---|---|---|
| 3303 | 3268 | 3301 | 3293 |
| 2919 | 2918 | 2923 | 2924 |
| 1657 | 1642 | 1646 | 1646 |
| 1481 | 1459 | 1459 | 1454 |
| 1013 a* | 1016 a* | 1018 b | 1022 b |
| 854 | 854 | 853 | 854 |
| 567 | 536 | 531 | – |

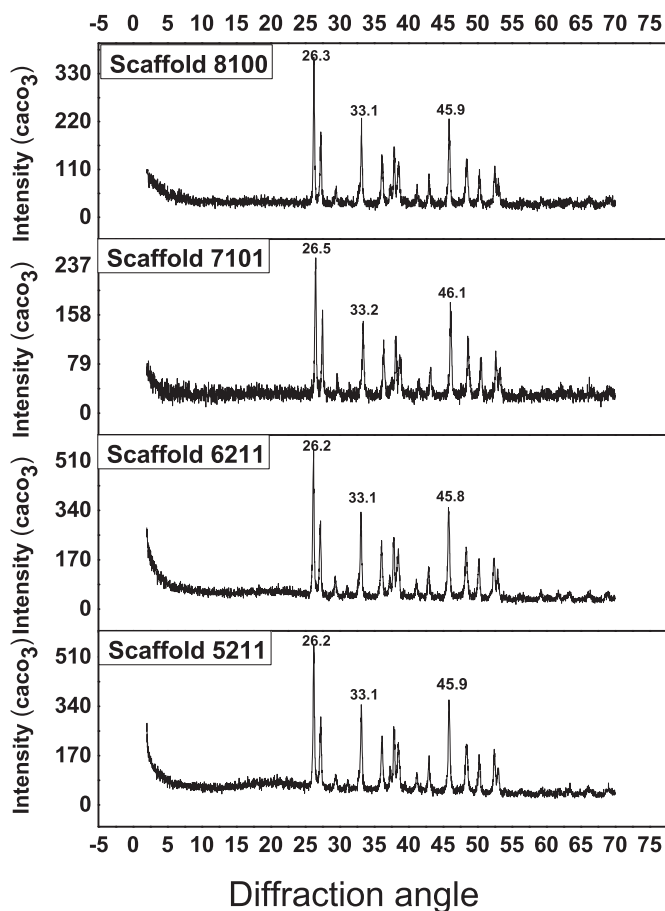The means with similar letters are not significantly different.



**Fig. 15.** X-ray diffraction analysis and the strongest three peaks.

**Table 5**
Briefing of the structural of caco3 at different percentage in the scaffolds composition.

| The scaffold | $2\theta \pm 0.001$ | $FWHM \pm 0.001$ | d (nm) | $D_{XRD}$ (nm) | $D_{TEM}$ (nm) |
|---|---|---|---|---|---|
| Scaffold 5211 (50%) | 26.2245 | 0.21550 | 33.9549 | 37.9 | 37.75 ± 3 |
| | 33.1189 | 0.23790 | 27.0271 | 34.8 | |
| | 45.8562 | 0.22290 | 19.7728 | 38.7 | |
| Scaffold 6211 (60%) | 26.1714 | 0.23380 | 34.0226 | 34.9 | 47.89 ± 8 |
| | 33.0731 | 0.22140 | 27.0635 | 37.4 | |
| | 45.8004 | 0.26280 | 19.7956 | 32.8 | |
| Scaffold 7101 (70%) | 26.4774 | 0.24100 | 33.6363 | 33.9 | 48.56 ± 6 |
| | 33.8732 | 0.23150 | 28.1443 | 35.9 | |
| | 46.09260 | 0.22190 | 19.6769 | 38.9 | |
| Scaffold 8100 (80%) | 26.2486 | 0.19070 | 33.9243 | 42.8 | 55.22 ± 9 |
| | 33.1444 | 0.20880 | 27.0069 | 39.7 | |
| | 45.8725 | 0.20760 | 19.7661 | 41.6 | |

happens between ions in a compound substance [12,30,33,49]. In our study, the interaction of calcium ions provided by ACN powder with the carboxyl groups in the gelatin is possibly the contributing factor. These results were very obvious and interpretable via the FTIR analysis.

The swelling performance of a scaffold improves its pore size [30,32,33,47]. Swelling performance is an additional factor a scaffold can provide. It has a practical use in supporting the attachment and growth of cells and the subsequent new tissue regeneration [44,50]. Swelling ratio of scaffolds is an average of slightly above 50% of medium absorption ability during the first 10 min. In this study the scaffolds 6211 and 7200 were observed to have such a ratio, while scaffolds 5211, 5400, 6300, 7101 and 8100 showed the lowest medium absorption ability on an average of less than 50%. These results were in disagreement with those of previous study by [35] who reported that higher swelling rates are positively related to the higher porosity of a scaffold. Nevertheless, [36] reported that swelling ratio was decreased when the scaffold is designed as nanocomposite structure similar to those fabricated in this study. One probable interpretation for this reduction may be attributed to the increase surface area of interaction of ACN with the gelatin, dextrin and dextran networking and its enhanced bonding properties. Unexpectedly, the investigations in this study showed that the swelling rate was significantly increased with the amount of gelatin, dextrin and dextran used in the combinations mixture. In addition, the porosity percentage was found to be significantly increased with increase in ACN powder content.

Degradation behavior of the polymer based scaffolds is another essential aspect in the area of tissue engineering. Biodegradability is primarily initiated by polymer chain back bone hydrolysis and to a minor extent via enzymatic activity [6]. Scaffold's weight loss increases from pure to high content during incubation period [51,52]. Studies on the degradation of the scaffolds showed comparable development as of the swelling ratio [30,32,33]. Positive relationship was investigated between the swelling performance and the degradation rate for scaffold 6211, 6300 and 7200 [30,32,33]. The later showed the highest degradation rate. However, scaffold 5211 showed the lowest degradation rate during both the enzymatic degradation study and the semiquantitative study [30,32,33]. All the studied scaffolds, except 6211 showed intermediate results when compared with scaffold 5211 being more advantageous for bone tissue engineering applications [30,32,33]. In this study enzymatic degradation investigation was presented as a short term observation based on the nature of lysozyme enzymes. Lysozyme enzymes break down the linkage groups of the gelatin, dextran and dextrin network [6]. The enzymatic degradation experiment showed that the breakdown of linkages between the gelatin, dextran and dextrin networking was accelerated as direct result of the raise in fluid uptake. Therefore, the loss of networking structure was initiated within few days of soaking. There was a positive relationship between the degradation time and the chain scission that results in decreasing the modulus values [52]. The structural reliability, constancy and the high concentration of gelatin led to degradation offset up to 14 days of the experimental period. A common characteristic of scaffolds can be a degradation rate that is balanced, in other words, neither too fast nor too slow for it to be rendered practical. Many factors that affect degradation time include polymer crystallinity, thermal history, molecular weight, porosity, monomer concentration, the location of the implant and geometry [6].

The osteoblast is such a cell that is vulnerable to pH changes and the acidity of the surrounding environment. In addition, pH is a significant factor that affects the electrical charges of the incubation solution [29]. The degradation of gelatin, dextran and dextrin polymers results in decline in pH values. Such change of pH has been reported to significantly lower osteoblast activity, ALP activity and collagen synthesis [6]. We theorized that the leaching of ACN powder from the gelatin, dextran and dextrin matrices throughout the degradation time results in an increase in the primary pH value of the solution toward more alkaline environment. Such situation may be associate or
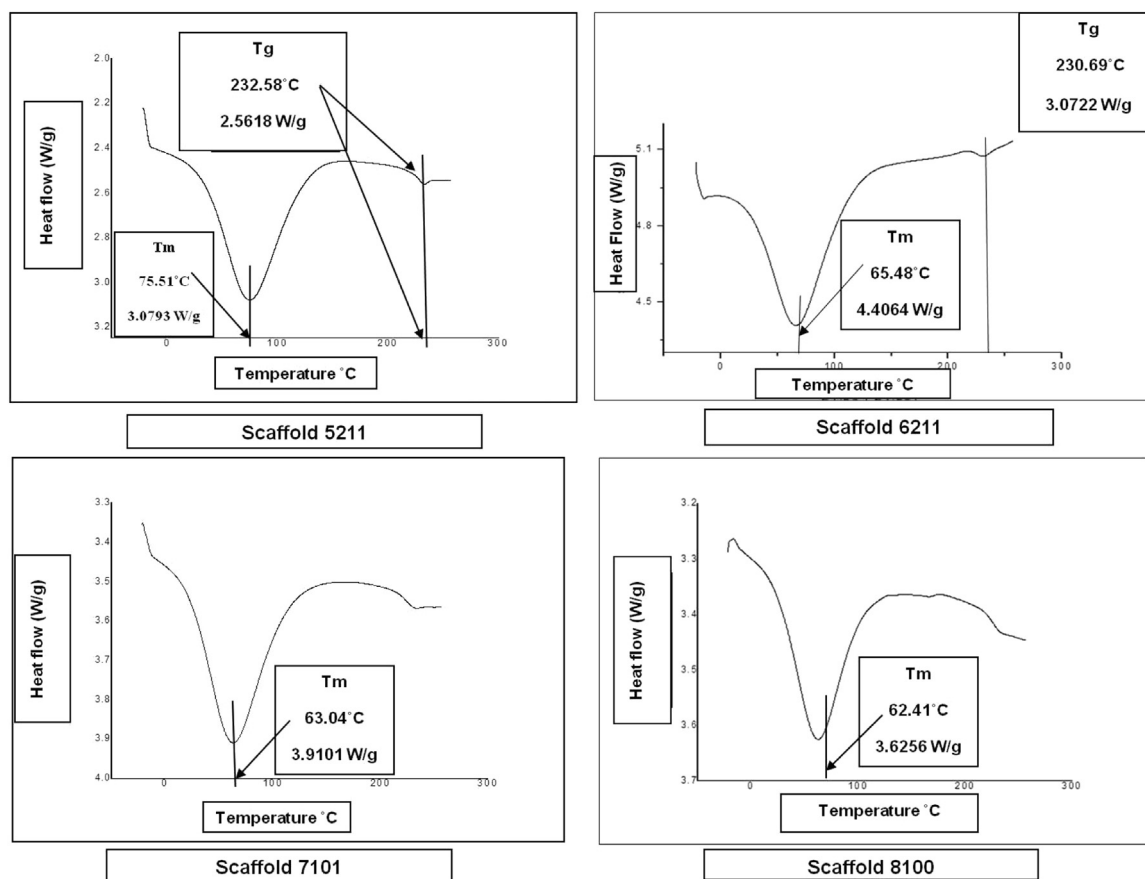
**Fig. 16.** The graphs show the endothermic DSC peak (denaturation) of the scaffold materials (gelatin, dextran, dextrin and ACN powder).

related to the concentration of ACN powder in the scaffolds. This alkalinizing and neutralizing effect of ACN powder towards the potential acidification (low pH) of the solution during gelatin, dextran and dextrin degradation creates an ideal mixture for bone grafting functions. Additionally, previous studies have reported a raise in osteoblast activity and fracture healing speed via metabolic alkalosis and/or acidosis [6]. This explains positive side of the raised pH of all degrading scaffolds under the study.

Chemical interaction investigation of the substances in the scaffold nanocomposite is a vital aspect that can assist in the adjustment and improvement of the scaffold properties. Studies such as FTIR, XRD, and DSC are useful means in understanding the physiochemical properties of the substances as well as the chemical interactions. In this study, the FTIR spectra study of the scaffolds was obvious that scaffolds 5211, 6211, 7101 and 8100 presented with a similar pattern of spectra. This is due to the existences of same substances in varying composition. The difference may be attributed to the sharpness and broadness of the peaks formed. These changes or differences were found to be related to the increasing amount of ACN powder in the scaffolds. Moreover, the increasing ACN powder quantity may designate the development of the ionic interaction between the positive charge of calcium ions and the negative charge of the carboxyl group of gelatin, dextrin and dextran [27,29,30,33,35,53]. Indeed, this ionic interaction is the factor that attributed to many scaffold characteristics such as mechanical properties and degradation behaviors.

The XRD analysis revealed important information on the mineral phase of the components of the scaffolds. The obtained spectra revealed characteristic aragonite peaks. Previous studies of [30,33,53–56] also reported the existences of dominant peaks characteristic of aragonite at 26.5 and 46.1 similar to those observed in this study. It appeared that all scaffolds that have ACN powder also have the aragonite form of calcium carbonate. This aragonite form was presented as the only

mineral phase presented in the scaffolds with no impurities or other substance created through the development procedure. On the other hand, the intensity of the peaks well matched ACN contained in all scaffold.

The DSC assessment of the developed scaffolds revealed essential information pertaining to the characteristics of the ideal scaffolds that served as guideline for selection of the best composition for advanced studies. The DSC was used to investigate the physical transformations or phase transitions of the nanocomposite scaffolds. Melting or glass transition temperatures of the substance were thus determined. The latter, provided an indication of the physical nature of these scaffolds. The melting Temperature ($T_m$) is great when the substances used are crystalline or semi-crystalline [32]. When a glassy state and the stage of glass transition are followed by significant reduction in the graph without other peaks been present, an average glass transition Temperature ($T_g$) can be determined [52]. Through its melting, the substance mixture showed two peaks close to each other. The peak found at 62.41–75.51 °C was attributed to gelatin, dextrin, and dextran melting. These temperatures are close with those used to extrude the mixture. Additionally, there are smaller peaks approximately at 230.69–232.58 °C that possibly correlated to glass transition Temperature ($T_g$). When the temperature increases the sample eventually reaches its melting Temperature ($T_m$). The melting method results in an endothermic peak in the DSC curve. The capability to conclude transition temperatures and enthalpies (thermodynamics and chemistry) makes DSC an important tool in producing phase diagrams for different chemical systems. The outcomes of the DSC of this study were in agreement to those of [57,48,58,53,52,30,33]. Glass transitions Temperature ($T_g$) may happen as the temperature of an amorphous solid is increased. These transitions came out as a step in the baseline of the recorded DSC indicator. It is a result of sample heat changes ability and no formal phase of transform happened. As the temperature

increases, an amorphous solid will become less pasty. This transition only happens to polymers and makes them unique. The amorphous portion undergoes the glass transition only, and the crystalline portion undergoes melting only.

## 5. Conclusion

This study concluded that using an innovative mixture of calcium carbonate in the form of aragonite nanocockle shells powder and gelatin, dextrin and dextran is the utmost appropriate composition that may guarantee the achievement of the developed scaffold purposes in true biological system. This innovative mixture also was essential in achieving the porous structure of the scaffolds that determined their successive characteristics. Of all, scaffold 5211 reached a tipping point in terms of ideal morphology, optimal physiochemical properties, and great mechanical strength. In addition, it expected very good cell attachment, distribution and growth rate compared to the other developed scaffolds in this study. Cell attachment analysis were done and the research paper submitted for publishing and in vivo evaluations are being carried out in our laboratory to fulfill all the major necessities to be considered as a bone replacement.

## Authors' contributions

All authors read and approved the final manuscript.

## Acknowledgements

## Appendix A. Transparency document

Transparency document associated with this article can be found in the online version at http://dx.doi.org/10.1016/j.bbrep.2017.04.008.

## References

[1] M.E. Oest, K.M. Dupont, H.J. Kong, D.J. Mooney, R.E. Guldberg, Quantitative assessment of scaffold and growth factor-mediated repair of critically sized bone defects, J. Orthop. Res. (2007) 941–950.

[2] K.A. Blackwood, N. Bock, T.R. Dargaville, M.A. Woodruff, Scaffolds for growth factor delivery as applied to bone tissue engineering: review article, Int. J. Polym. Sci. 2012 (2012) 1–25.

[3] U. Kneser, D.J. Schaefer, E. Polykandriotis, R.E. Horch, Tissue engineering of bone: the reconstructive surgeon's point of view, J. Cell. Mol. Med. 10 (1) (2006) 7–19.

[4] M. Pilia, T. Guda, M. Appleford, Development of composite scaffolds for load-bearing segmental bone defects, BioMed. Res. Int. 2013 (2013) 1–15.

[5] A.W. Blom, J.L. Cunningham, G. Hughes, T.J. Lawes, N. Smith, G. Blunn, I.D. Learmonth, A.E. Goodship, The compatibility of ceramic bone graft substitutes as allograft extenders for use in impaction grafting of the femur, J. Bone Jt. Surg. 87-B (3) (2005) 421–425.

[6] M. Navarro, A. Michiardi, O. Castaño, J.A. Planell, Biomaterials in orthopaedics, J. R. Soc. Interface 5 (27) (2008) 1137–1158.

[7] A.S. Brydone, D. Meek, S. Maclaine, Bone grafting, orthopaedic biomaterials, and the clinical need for bone engineering, J. Eng. Med. 224 (2010) 1329.

[8] A. Anvari-Yazdi, A. Yazdani, T. Talaei-Khozani, M. Kalantar, Extraction and viability checking of various carbonated hydroxyapatite by Whartons' Jelly Mesenchymal stem cell, Sci. Int. 1 (5) (2013) 1–6.

[9] J. Han, Z. Zhou, R. Yin, D. Yang, J. Nie, Alginate chitosan/hydroxyapatite polyelectrolyte complex porous scaffolds: preparation and characterization, Int. J. Biol. Macromol. 46 (2) (2010) 199–205.

[10] K. Venkateswarlu, D. Sreekanth, M. Sandhyarani, V. Muthupandi, A.C. Bose, N. Rameshbabu, X-ray peak profile analysis of nanostructured hydroxyapatite and fluorapatite, Int. J. Biosci. Biochem. Bioinforma. 2 (6) (2012) 389–393.

[11] C. Suryanarayana, M.G. Norton, X-Ray Diffraction: A Practical Approach, Plenum Press Publishing, New York, 1998.

[12] A. Bernhardt, A. Lode, F. Peters, M. Gelinsky, Novel ceramic bone replacement material osbone® in a comparative in vitro study with osteoblasts, Clin. Oral.

[13] Implants Res. 22 (6) (2011) 651–657.

[13] C.A. Smith, S.M. Richardson, M.J. Eagle, P. Rooney, T. Board, J.A. Hoyland, The use of a novel bone allograft wash process to generate a biocompatible, mechanically stable and osteoinductive biological scaffold for use in bone tissue engineering, J. Tissue Eng. Regen. Med. (2014) (published by John Wiley and Sons Ltd.).

[14] A.M. Jakoi, J.A. Iorio, P.J. Cahill, Autologous bone graft harvesting: a review of grafts and surgical techniques, Musculoskelet. Surg. 99 (3) (2015) 171–178.

[15] S.K. Nandi, R.P. Mukherjee, B. Kundu, D.K. De, D. Basu, Orthopaedic applications of bone graft and graft substitutes: a review, Indian J. Med. Res. 132 (2010) 15–30.

[16] K. Lee, E. Silva, D. Mooney, Growth factor delivery-based tissue engineering: general approaches and a review of recent developments, J. R. Soc. Interface 8 (55) (2011) 153–170.

[17] S. Bose, M. Roy, A. Bandyopadhyay, Recent advances in bone tissue engineering scaffolds, Trends Biotechnol. 30 (10) (2012) 546–554.

[18] A. Bernhardt, F. Despang, A. Lode, A. Demmler, T. Hanke, M. Gelinsky, Proliferation and osteogenic differentiation of human bone marrow stromal cells on alginate-gelatine-hydroxyapatite scaffolds with anisotropic pore structure, J. Tissue Eng. Reg. Med. 3 (1) (2009) 54–62.

[19] M. Rajkumar, N. Meenakshisundaram, V. Rajendran, Development of nanocomposites based on hydroxyapatite/sodium alginate: synthesis and characterization, Mater. Charact. 62 (5) (2011) 469–479.

[20] A.F. Lemos, J.H.G. Rocha, S.S.F. Quaresma, S. Kannan, F.N. Oktar, S. Agathopoulos, J.M.F. Ferreira, Hydroxyapatite nano-powders produced hydrothermally from nacreous material, J. Eur. Ceram. Soc. 26 (16) (2006) 3639–3646.

[21] M. Kanitkar, H.D. Tailor, W.S. Khan, The use of growth factors and Mesenchymal stem cells in orthopaedics, Open Orthop. J. 5 (2011) 271–275.

[22] A.B.Z. Zuki, Z. Norazri, K. Zaleha, Mineral composition of the cockleshell (Anadora granosa) shells, hard clamp (Meretrix meretrix) shells and corals (Porites spp): comparative study, J. Anim. Vet. Adv. 3 (2004) 445–447.

[23] A.J. Awang-Hazmi, A.B.Z. Zuki, M.M. Noordin, A. Jalila, Y. Norimah, Mineral composition of the cockle (Anadara granosa) shells of west coast of Peninsular Malaysia and its potential as biomaterial for use in bone repair, J. Anim. Vet. Adv. 6 (5) (2007) 591–594.

[24] K.H. Islam, A.B.Z. Zuki, M.M. Noordin, M.H. Zobir, N.S. Abd Rahman, M.E. Ali, Characterization of calcium carbonate and its polymorphs from cockle shells (Anadara granosa), J. Powder Technol. 213 (1–3) (2011) 188–191.

[25] K.H. Islam, A.B.Z. Zuki, M.E. Ali, M.Z.B. Hussein, M.M. Noordin, M.Y. Loqman, H. Wahid, M.A. Hakim, S.B.A. Hamid, Facile synthesis of calcium carbonate nanoparticles from cockle shells: research article, J. Nanomater. 2012 (2012) 1–5.

[26] K.H. Islam, A.B.Z. Zuki, M.E. Ali, M.H. Zobir, M.M. Noordin, M.Y. Loqman, G. Miah, H. Wahid, U. Hashim, A novel method for the synthesis of calcium (aragonite) nanoparticles from cockle shells, J. Powder Technol. (2013) 70–75.

[27] M.E. Hoque, M. Shehryar, K.M.N. Islam, Processing and characterization of cockle shell calcium carbonate (caco3) bioceramic for potential application in bone tissue engineering, J. Mater. Sci. Eng. 2 (4) (2013) 1–5.

[28] J. Lee, M.J. Cuddihy, N.A. Kotov, Three-dimensional cell culture matrices: state of the art, Tissue Eng. 14 (1) (2008) 61–86.

[29] K. Wang, C. Zhou, Y. Hong, X. Zhang, A review of protein adsorption on bioceramics, J. Interface Focus 2 (3) (2012) 259–277.

[30] H. Bharatham, B.Z. Zuki, E.K. Perimal, M.Y. Loqman, M. Hamid, Mineral and physiochemical evaluation of Cockle shell (Anadara granosa) and other selected molluscan shell as potential biomaterials, Sains Malays. 43 (7) (2014) 1023–1029.

[31] E.A. Hager, Composite Gelatin Delivery System for Bone Regeneration, DBS. Massachusetts Institute of Technology, 2004.

[32] F.H. Bahaa, Fabrication of Cockle (Anadara granosa) – Shell Based 3D-Scaffold for Bone Repair (Thesis for the degree of doctor of philosophy), UPM, 2010.

[33] H. Bharatham, B.Z. Zuki, E.K. Perimal, M.Y. Loqman, M. Hamid, Development and characterization of novel porous 3d alginate-cockle shell powder nanobiocomposite bone scaffold: research article, BioMed. Res. Int. 2014 (2014) 1–12. 146723.

[34] A. Shahini, M. Yazdimamaghani, K.J. Walker, M.A. Eastman, H. Hatami-Marbini, B.J. Smith, J.L. Ricci, S.V. Madihally, D. Vashaee, L. Tayebi, 3D conductive nanocomposite scaffold for bone tissue engineering, Int. J. Nanomed. 9 (2014) 167–181.

[35] S. Soumya, K.M. Sajesh, R. Jayakumar, S.V. Nair, K.P. Chennazhi, Development of a phytochemical scaffold for bone tissue engineering using Cissus quadrangularis extract, Carbohydr. Polym. 87 (2) (2012) 1787–1795.

[36] M. Peter, N.S. Binulal, S. Soumya, Nanocomposite scaffolds of bioactive glass ceramic nanoparticles disseminated chitosan matrix for tissue engineering applications, Carbohydr. Polym. 79 (2) (2010) 284–289.

[37] S.G. Le´vesque, R.M. Lim, M.S. Shoichet, Macroporous interconnected dextran scaffolds of controlled porosity for tissue- engineering applications, Biomaterials 26 (2005) 7436–7446.

[38] C. Vater, A. Lode, A. Bernhardt, A. Reinstorf, C. Heinemann, M. Gelinsky, Influence of different modifications of a calcium phosphate bone cement on adhesion, proliferation, and osteogenic differentiation of human bone marrow stromal cells, J. Biomed. Mater. Res. 92 (4) (2010) 1452–1460.

[39] M. Maria, A. E-G, Bone Tissue Engineering Strategy Basal on Starch Scaffolds and Bone Marrow Cells Cultured in a Flow Perfusion Bioreactor (Ph.D. thesis), Universi dade Do Minho Escola De Engenharia, 2004.

[40] H.G. Kang, S.Y. Kim, Y.M. Lee, Novel porous gelatin scaffolds by overrun/particle leaching process for tissue engineering applications, J. Biomed. Mater. Res. 79B (2006) 388–397.

[41] R. Dittrich, G. Tomandl, F. Despang, A. Bernhardt, Th Hanke, W. Pompe, M. Gelinsky, Scaffolds for hard tissue engineering by ionotropic gelatin of alginate-influence of selected preparation parameters, J. Am. Ceram. Soc. 90 (6) (2007) 1703–1708.

[42] B. Duan, M. Wang, Customized Ca-P/PHBV nanocomposite scaffolds for bone tissue engineering: design, fabrication surface modification and sustained release of growth factor, J. R. Soc. Interface (2010) 1–15.

[43] K.C.R. Kolan, M.C. Leu, G.E. Hilmas, T. Comte, Effect of architecture and porosity on mechanical properties of borate glass scaffolds made by selective laser sintering, Rapid Prototyp. J. 65 (2013) 816–826.

[44] F. Tavangarian, R. Emadi, Preparation of bioactive nanostructure scaffold with improved compressive strength, Ceram.-Silikáty 55 (1) (2011) 49–53.

[45] W.D. Xiao, Z.M. Zhong, Y.Z. Tang, Z.X. Xu, Z. Xu, Repair of critical size bone defects with porous poly (D,L-Iactide)/nacre nanocomposite hollow scaffold, Saudi Med. J. 33 (6) (2012) 601–607.

[46] N. Sagar, A.K. Pandey, D. Gurbani, K. Khan, D. Singh, B.P. Chaudhari, V.P. Soni, N. Chattopadyay, A. Dhawan, J.R. Bellare, In-vivo efficacy of compliant 3D nano-composite in critical-size bone defect repair: a six month preclinical study in rabbit, PLoS One 8 (10) (2013) e77578, ⟨www.plosone.org⟩.

[47] Y. Zhang, J. Wang, J. Wang, X. Niu, J. Liu, L. Gao, X. Zhai, K. Chu, Preparation of porous PLA/DBM composite biomaterials and experimental research of repair rabbit radius segmental bone defect, Cell Tissue Bank. 16 (4) (2015) 615–622.

[48] M.G. Haugh, The Development of Novel Scaffolds for Tissue Engineering With a Range of Structural and Mechanical Properties (Ph.d. thesis), University of Dublin, Trinity College, Dublin, 2009.

[49] W. Gu, C. Wu, J. Chen, Y. Xiao, Nanotechnology in the targeted drug delivery for bone diseases and bone regeneration, Int. J. Nanomed. 8 (2013) 2305–2317.

[50] Z. Li, H.R. Ramay, K.D. Hauch, D. Xia, M. Zhang, Chitosan–alginate hybrid scaffolds for bone tissue engineering, Biomaterials 26 (2005) 3919–3928.

[51] M.H. Ardakani, F. Kavian, F. Moztarzadeh, M. Eslaminejad, A. Zamanian, F. Bagheri, Poly (lactic-co-glycolic)/nanostructured merwinite porous composites for bone tissue engineering. I. Preparation and morphology, Key Eng. Mater. (2012) 718–722.

[52] H. Fouad, T. Elsarnagawy, F.N. Almajhadi, K.A. K.A. Khalil, Preparation and In vitro thermo-mechanical characterization of electrospun PLGA nanofibers for soft and hard tissue replacement, Int. J. Electrochem. Sci. 8 (2013) 2293–2304.

[53] M. Mohamed, S. Yusup, S. Maitra, Decomposition study of calcium carbonate in cockle shell, J. Eng. Sci. Technol. 7 (1) (2012) 1–10.

[54] A. Behnamghader, N. Bagheri, B. Raissi, F. Moztarzadeh, Phase development and behavior of biphasic HA-TCP calcium phosphate materials prepared from hydro-xyapatite and bioactive glass, J. Mater. Sci: Mater. Med. 9 (1) (2008) 197–201.

[55] T. Mass, J.L. Drake, L. Haramaty, Y. Rosenthal, O.M.E. Schofield, R.M. Sherrell, P.G. Falkowski, Aragonite precipitation by "proto-polyps" in coral cell cultures, PLoS ONE 7 (4) (2012) e35049, ⟨www.plosone.org⟩.

[56] C. Moseke, M. Gelinsky, J. Groll, U. Gbureck, Chemical characterization of hydroxyapatite obtained by wet chemistry in the presence of V, Co, and Cu ions, J. Mater. Sci. Eng. 33 (3) (2013) 1654–1661.

[57] M. Marcos, S. da Paula, B.B. Fabiana, R. Medeiros, M.B. Adriano, A.F. M´arcio, A. El´idio, Characterization of aluminized polyethylene blends via mechanical recycling, Mater. Sci. Eng. A 403 (2005) 37–41.

[58] S. Thumsorn, K. Yamada, Y.W. Leong, H. Hamada, Development of cockle shell-derived caco3 for flame retardancy of recycled PET/recycled PP blends, Mater. Sci. Appl. 2 (2011) 59–69.